Fatigue life modelling under variable amplitude multiaxial loading: Comparison between fatigue criterion and incremental modelling

Fabricio Dal Cero Coelho, Quochuy Vu, Damien Halm, Yves Nadot

Fatigue life modelling under variable amplitude multiaxial loading: comparison between fatigue criterion and incremental modelling

F. Dal Cero Coelho, Q.H. Vu, D. Halm, Y. Nadot

PII: S0142-1123(18)30382-7
DOI: https://doi.org/10.1016/j.ijfatigue.2018.08.013
Reference: JIJF 4809

To appear in: *International Journal of Fatigue*

Received Date: 20 April 2018
Revised Date: 7 August 2018
Accepted Date: 11 August 2018

Please cite this article as: Dal Cero Coelho, F., Vu, Q.H., Halm, D., Nadot, Y., Fatigue life modelling under variable amplitude multiaxial loading: comparison between fatigue criterion and incremental modelling, *International Journal of Fatigue* (2018), doi: https://doi.org/10.1016/j.ijfatigue.2018.08.013

Fatigue life modelling under variable amplitude multiaxial loading: comparison between fatigue criterion and incremental modelling

F. Dal Cero Coelho[a], Q. H. Vu[b], D. Halm[a,*], Y. Nadot[a]

a: Institute Pprime (UPR 3346), CNRS, ENSMA, Université de Poitiers, Chasseneuil, France

b: Hanoi University of Science and Technology, School of Transportation Engineering, Hanoi, Vietnam

*: corresponding author, damien.halm@ensma.fr, tel.: +33549498231, fax: +33549498238

Abstract

This study deals with fatigue of a 1045 carbon steel subjected to a cyclic tension-torsion spectrum combining in-phase and out-of-phase loadings and including overload, representative of an automotive chassis loading type. The experimental lifetimes are compared to the results of two different approaches. The first one combines a multiaxial fatigue criterion able to describe out of phase loading and a non-linear damage rule. The second one is based on an incremental mesoscale plasticity/damage model. It is shown that the criterion involving a non-linear damage rule is able to describe the experimental result for full spectrum (with overload) but the identification of the non-linearity is a function of spectrum type. The incremental approach gives better results for both spectra (with and without overloads) and does not need specific parameter identification.

1 Introduction

In the sector of automotive engineering, the car-to-ground connecting components undergo multiaxial cyclic loading. Usual loading corresponds to « smooth » driving on a well-maintained road and is in the range of High Cycle Fatigue (10^6-10^8 cycles), as well as turns or driving on cobblestones, which are however more demanding. Events in the range of Low Cycle Fatigue (1-10^4 cycles) may happen, for example impacts of potholes on wheels. The complexity of automotive fatigue loadings is taken into account by combining different types of multiaxial loadings, representative of in service stresses. In order to forecast lifetime of industrial components, reliable tools capturing the effects of multiaxiality and damage accumulation are needed. This complex topic has been addressed by researchers over the past 50 years with different types of modelling strategies, starting from very simple linear analysis up to complex nonlinear modelling, including different scales or methodologies. A short

summary of major approaches is presented in this introduction, which is of course not exhaustive as many different modellings are available to address the problem, in terms of both fatigue criteria (approaches by critical planes [1-4], by integrals, [5-7], by stress invariants [8-11], by energetic considerations [12,13]) and damage accumulation (linear [14], nonlinear [15,16], by damage curve [17])

One of the simplest approach to solve the question of fatigue life under variable amplitude and complex multiaxial loading is to define an equivalent stress (criterion) to describe the multiaxial stresses and to perform linear accumulation damage. Most of the fatigue criteria are addressing the question of multiaxial stresses under proportional loadings with variable accuracy, especially when loadings include pure biaxiality and different load ratios. This general simple approach is not able to capture out of phase and frequency shift effects as well as nonlinear damage accumulation.

As a second step, the description of the loading complexity can be improved by integrating out of phase effect or shift frequency. Several criteria are able to deal with non-proportional loadings and already compared to experiments. The cost to be paid for this improvement leads, most of the time, to additional complexity for the criterion calculation and needs additional fatigue data. An accurate evaluation of in service fatigue life of a real component needs such level of complexity.

A third step is to improve the damage accumulation rule by taking into account nonlinear effects that are already very well-known from the experimental viewpoint but strongly material dependent. For that purpose, a nonlinear damage accumulation law is necessary and most of the time this is closely related to the material and the spectrum. It seems that no general simple approaches can deal accurately with nonlinear damage accumulation without being strongly correlated to the spectrum type. This third step of improvement corresponds to a relatively advanced method for the point of view of the design engineer and is able to solve most of the fatigue design issues but necessitates a good knowledge of the material's fatigue behavior under complex spectrum.

Another totally different approach is to link each cycle to a given level of damage. Most of the time incremental modellings are based on Thermodynamics of Irreversible Process and the load history is implicitly included in the damage internal variables so that no specific parameter for loading history is needed to describe nonlinear accumulation damage. Advanced approaches are using scale transition in the high cycle fatigue range with local plasticity and damage at the local scale in order to describe fatigue mechanisms in the HCF range (macroscopic elasticity, plasticity and damage at the local scale). This type of approach

is not so popular in the fatigue literature, probably due to a higher complexity of the identification procedure and higher computational cost for a real complex component, but should be further developed because of the direct capability of the method to describe complex loading.

While, as indicated above, one may find in the literature more or less complex approaches to predicting the in service lifetime of components subjected to high cycle fatigue, publications generally do not compare the different theories and their performance on a single material, whose behaviour has been clearly identified, and on multi-axial loading cases representative of in service use. The work presented here aims to fill this gap. It deals with a unique, widely used material, a 1045 carbon steel subjected to a specific tension-torsion loading. This spectrum combines in-phase and out-of-phase loadings, with different load ratios and includes overloadings exceeding the yield stress. In a first part, the fatigue lifetimes are measured and the damage mechanisms are observed and interpreted. The lifetimes are then compared to the results of different modelling methodologies: (1) approaches based on stress invariants [8,18] are selected, owing to their reliability, their simple use and their reasonable computing time and then associated with different damage accumulation rules (Miner linear accumulation [14], « DCA » non linear accumulation [17]), and (2) the damage model by Vu [19]. The aim is to evaluate the respective capabilities of each of these approaches in terms of the reliability of the results.

2 Material and experimental conditions

In this section, the material is first presented. A 1045 carbon steel is selected because a lot of information about this material can be found in the literature. Then, the complex loading spectrum representative of stresses undergone by car-to-ground components is detailed. It comprises the effects of paved roads, curves and shocks on the wheels.

2.1 Material characteristics

The material is a 1045 carbon steel, used in many industrial applications. It has been the subject of many previous studies from the authors of the present paper [19-24]. The main

mechanical characteristics are a Young's modulus E = 205 GPa, a monotonous yield stress $R_{p0.2\ monotonous}$ = 350 MPa, a cyclic yield stress $R_{p0.2\ cyclic}$ = 280 MPa and an ultimate stress R_m = 580 MPa. This steel alternates ferrite and pearlite bands, the average grain size is 22 µm for ferrite and 16 µm for pearlite (a micrography can be seen in Figure 7). The chemical composition of the 1045 steel is given in [19].

The cylindrical tested specimens, whose minimum diameter is 9 mm, were machined from a round bar (diameter 80 mm). The specimen axis corresponds to that of the bar, *i.e.* the rolling axis. In order to observe the cracks at microscopic scale (5 – 10 µm), the specimens were polished with several abrasive papers up to grade 4000. Then, the samples were tempered at 500 °C during one hour under vacuum to remove the residual stress due to the preparation stage of specimens.

2.2 Experimental procedure - Variable amplitude loading

Tests were performed on a servo-hydraulic axial – torsional machine (Instron type 1343) at room temperature and under ambient air. Applied normal stress amplitude σ_a and shear stress amplitude τ_a were calculated according to the following equations: $\sigma_a = 4F/\pi d^2$, $\tau_a = 16T/\pi d^3$, where F is the tension force, T is the torque and d is the minimum section diameter of the specimen. The replica technique [25] applied on the external specimen surface was used to monitor crack initiation and propagation. A soft dental resin is put on the specimen by the means of a mold. This allows recording and observing the surface of the specimen without disassembling and reassembling of the set-up. After metallization, the replicas were observed under SEM with low acceleration voltage. The procedure of observation starts with the last replica where the principal crack can be easily identified, and comes back to the early stages of cracking. The replica is a negative image of real surface. Resolution of this technique is about 5 – 10 µm depending on the crack opening.

The loading spectrum (Figure 1) used in tension-torsion tests is designed to represent a simplification of the real fatigue loadings undergone by in-service automotive structures.

The "Belgian Blocks (BB)" represent the effect of a paved road. The low mean stress in these blocks stands for the vehicle weight. Their recurrence is high (76% of spectrum) and their intensity low/medium. Note that the tension and torsion signals are out-of-phase, with a phase shift of 90°. The load ratio is -0.8 for tension and torsion. It represents

- The "Turns (TN)" represent the effect of the curves of the road. The strong

dissymmetry between the tension and torsion mean stress stands for the effect of the vehicle weight when turning. Their recurrence is medium (23% of spectrum) and their intensity low. Both signals are in-phase. The load ratio is -4.7 for tension, -0.2 for torsion.

- The "Shocks (SCK)" represent the effect of a shock on the wheel (impact due to pavement, for example). Both signals are in-phase, which assumes a simultaneous impact on both wheels. The loading levels in this block may lead to local plasticity. Their recurrence is low. The load ratio is -0.7 for tension and torsion.

The loading sequence comprises a first set composed of 5 "BB" (separated in BB1 and 2 depending on the sign of the phase shift) and followed by 12 "TN". This set is repeated 50 times. Then the specimen undergoes 2 "SCK". The whole sequence is then repeated as many times as necessary to break the specimen.

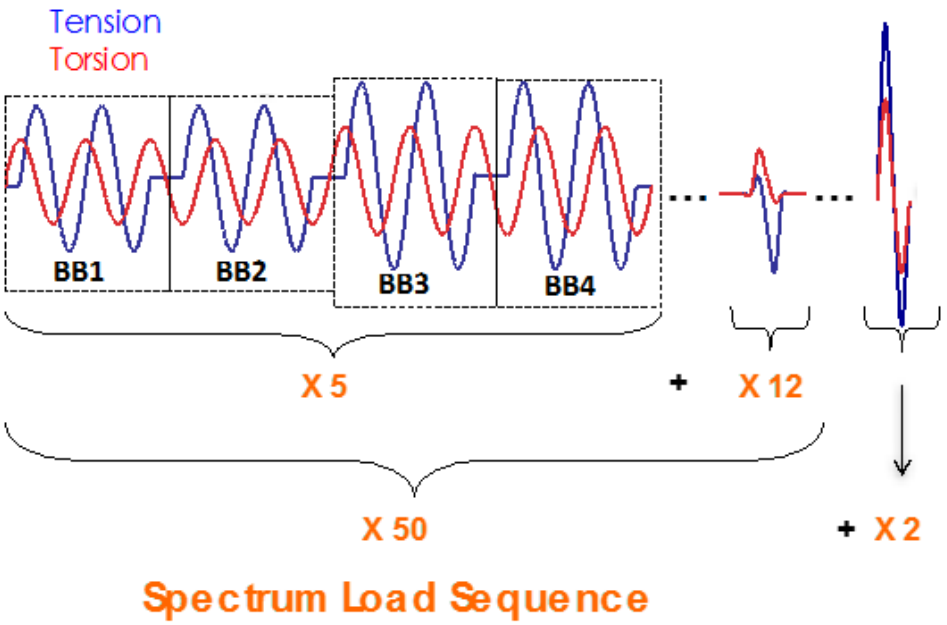

Figure 1 Spectrum for tension-torsion loadings

The spectrum reference parameter is the maximal von Mises stress in the "Shocks" block SCK; the amplitude of other blocks is defined by a ratio with respect to this reference stress level. Carrying out tests with a complex loading spectrum is a challenging task. In order to perform stable fatigue tension-torsion tests on a hydraulic device while keeping a reasonable test frequency, a preliminary study of the PID (proportional integral derivative

control) is necessary. After an optimization phase, PID values have been determined to ensure a satisfactory compromise between the set point monitoring and the test stability. The theoretical spectrum levels had to be corrected according to the real mean values recorded during the tests. That is the reason why Table 1 contains the "experimental" mean and amplitude values undergone by the specimen, which are slightly different from the theoretical values. In Table 1 and in the following, the test reference refers to the theoretical value. Σ_x is the applied tension component, Σ_{xy} the shear one and σ_{VM} the maximum Von Mises stress undergone during the "SCK" block. The test frequency for sinus loading is 3Hz for BB and 6Hz for TN and SCK.

Table 1 Experimental loading spectrum values: Stress amplitude and mean value per block

Test reference	Experimental value of σ_{VM} "SCK"	Stress component	Belgian Blocks BB1 – BB2	Belgian Blocks BB3 – BB4	Turns (TN)	Shocks (SCK)
600 MPa	526 MPa	$\Sigma_{x\ mean}$ [MPa]	19	25	-84	57
		$\Sigma_{x\ amplitude}$ [MPa]	174	222	125	355
		$\Sigma_{xy\ mean}$ [MPa]	11	18	45	19
		$\Sigma_{xy\ amplitude}$ [MPa]	100	129	58	169
525 MPa	504 MPa	$\Sigma_{x\ mean}$ [MPa]	17	21	-72	54
		$\Sigma_{x\ amplitude}$ [MPa]	151	195	108	311
		$\Sigma_{xy\ mean}$ [MPa]	11	13	40	28
		$\Sigma_{xy\ amplitude}$ [MPa]	91	116	57	172
480 MPa	463 MPa	$\Sigma_{x\ mean}$ [MPa]	13	17	-68	44
		$\Sigma_{x\ amplitude}$ [MPa]	140	179	102	288
		$\Sigma_{xy\ mean}$ [MPa]	10	12	38	28
		$\Sigma_{xy\ amplitude}$ [MPa]	83	106	49	157

3 Experimental fatigue lifetime and damage mechanisms under variable amplitude loading

The effect of "shocks" in the loading spectrum on the material lifetime is often neglected in industrial applications. Their influence can be very different according to the elastic-plastic

behavior, and strongly varies between a smooth or a notched sample [26,27]. The influence of the overloads is studied by analyzing the number of cycles to failure, the orientation of the critical planes and the evolution of fatigue cracks.

3.1 Fatigue lifetime under variable spectrum

For each test defined in Table 1, Table 2 provides the number of tension cycles undergone up to failure. The full spectrum sequence (Figure 1) contains 2602 tension cycles. Four specimens have been tested with a maximum theoretical von Mises stress of 525 MPa (one of them, noted "REPLICA" has been used to observe fatigue crack initiation and growth by the means of the replica technique), two with 600 MPa and two with 480 MPa. In order to analyze the effect of shocks on the fatigue lifetime, a simplified spectrum ("NO SHOCKS" in Table 2) has been tested, in which the "SCK" cycles have been suppressed. The results are presented in a figure providing the maximal experimental Von Mises stress in "shocks" blocks vs. the number of tension cycles to failure.

Table 2 Experimental results for spectra

Specimen Reference	σvm SCK Theoretical value [MPa]	σvm SCK Experimental value [MPa]	Number of tension cycles to failure
525_1	525	504	234 180
525_2	525	504	353 872
525_3	525	504	294 026
480_5	480	463	801 416
600_6	600	526	124 896
600_7	600	526	140 508
480_8	480	463	629 648
525_9_REPLICA	525	504	265 404
525_10_NO-SHOCKS	525	504	596 544
525_11_NO-SHOCKS	525	504	638 560
525_12_NO-SHOCKS	525	504	1 004 432

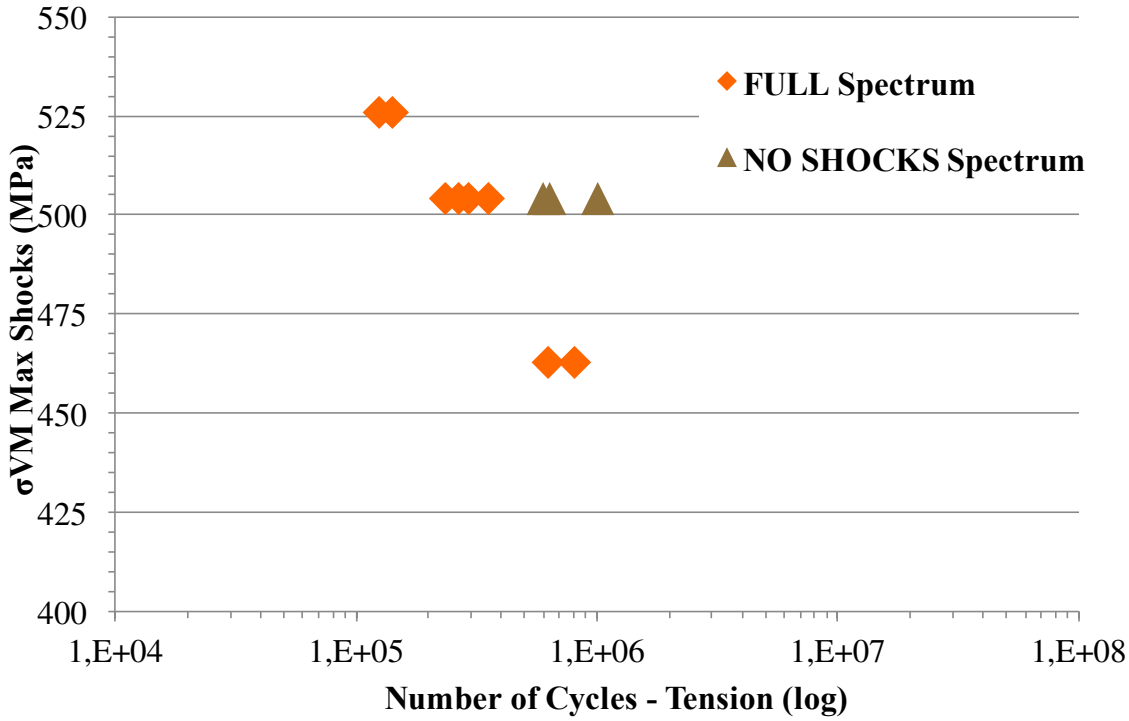

Figure 2 Comparison of lifetime with or without "shocks" blocks

Although the "SCK" blocks represent only 0,1% of total spectrum, a non-negligible impact of these cycles is observed on the fatigue lifetime of specimens. Mean fatigue lifetime for "NO SHOCKS" spectrum is around 60% greater than mean fatigue lifetime for "FULL" spectrum. This confirms the harmfulness of the SCK blocks pointed out by [26,28].

3.2 Initiation and propagation mechanisms

In order to understand the influence of each type of block depicted in the previous section, damage mechanisms are observed for "FULL" and "NO SHOCKS" spectrum. According to standard observations [22,29-31], the crack propagation splits into two stages. After the stage 1 occurring on the maximum shear planes (mode II/III – shear stress dominated), the cracks branch into planes of maximum normal stress (stage 2 – mode I – normal stress dominated). Orientation of these critical planes can be calculated by the damage accumulation method for each loading case [32]. Applied normal and shear stress are expressed as:

$$\Sigma_{xx}(t) = \Sigma(t) = \Sigma_{xm} + \Sigma_{xa}\sin(\omega t) \qquad (1)$$

$$\Sigma_{xy}(t) = \mathrm{T}(t) = \Sigma_{xym} + \Sigma_{xya}\sin\left(\omega t - \delta_{xy}\right) \qquad (2)$$

where stress tensor components $\Sigma_{xx}(t)$ and $\Sigma_{xy}(t)$ are expressed as a function of mean (respectively, amplitude) normal stress Σ_{xm} (respectively, Σ_{xa}) and mean (respectively, amplitude) shear stress Σ_{xym} (respectively, Σ_{xya}), time t, pulsation ω and the phase shift angle δ_{xy}. Figure 4 shows the definition of the angle α used to determine orientation of an arbitrary plane in the coordinate system associated to the specimen.

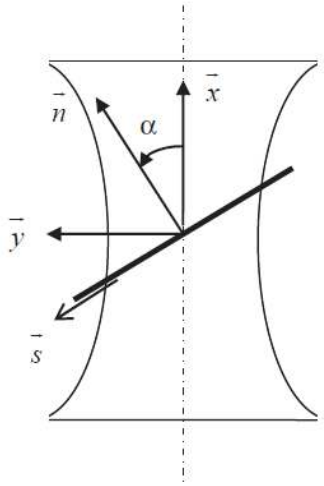

Figure 3 specimen schematization and definition of the angle α

Since cracks often initiate on the specimen surface, normal (σ_n) and shear (τ_{ns}) stress components on an arbitrary plane can be calculated under the hypothesis of plane stress as a function of the angle α (angle between the plane normal $\vec{n}$ and the specimen axis):

$$\sigma_n(t) = \Sigma(t)\cos^2\alpha + \mathrm{T}(t)\sin 2\alpha \qquad (3)$$

$$\tau_{ns}(t) = \mathrm{T}(t)\cos 2\alpha - \frac{1}{2}\Sigma(t)\sin 2\alpha \qquad (4)$$

The values of α ($-90° \le \alpha \le 90°$) corresponding to critical (maximal) shear plane ($\tau_{ns,\,max}$) and to critical (maximal) normal stress plane ($\sigma_{n,\,max}$) for each loading block mentioned in this work are shown in Table 3. The factor k represents the ratio of the shear and normal amplitude and is equal to 0.57 for all blocks.

Table 3 Calculated critical plane orientation

Block	δ_{xy} (°)	$k = \tau_a/\sigma_a$	$\alpha(\tau_{ns,\,max})$ (°)	$\alpha(\sigma_{n,\,max})$ (°)
Belgian Blocks	90 / -90	0.57	0 and 90	0

Turns	0	0.57	-20.6 and 69.4	24.4
Shocks	0	0.57	-20.6 and 69.4	24.4

Figure 4 presents the fatigue crack after the test at the surface for the specimen quoted "525_9_REPLICA" in Table 2. The replica of the specimen surface has been observed by SEM (

Figure 5) to measure experimental orientation of the crack planes and to compare it to the values calculated in Table 3. It can be noticed that the damage state is strongly localized: only one crack seems to initiate from a polishing scratch. It then propagates until about 95% (

Figure 5-g) of total lifetime in a plane close to the one maximizing the shear stress during the "BB" cycles (α=0). Note that at this stage no explicit influence of "Turns" and "Shocks" has been observed. A similar study performed by Vu et al. [19] showed that tension-torsion in-phase loadings with a stress ratio k = 0.5 (like "Turns" and "Shocks") lead to multiple initiation sites. However, when localized (like "BB") and diffuse (like "Turns" and "Shocks") modes are in competition, the localized one tends to govern crack propagation. At around 95% of total lifetime, a change in the direction of the crack path is observed: the angle between the normal to the crack propagation plane and the specimen axis is about -43°. This value does not correspond to any critical angle associated to the spectrum blocks (Table 3).

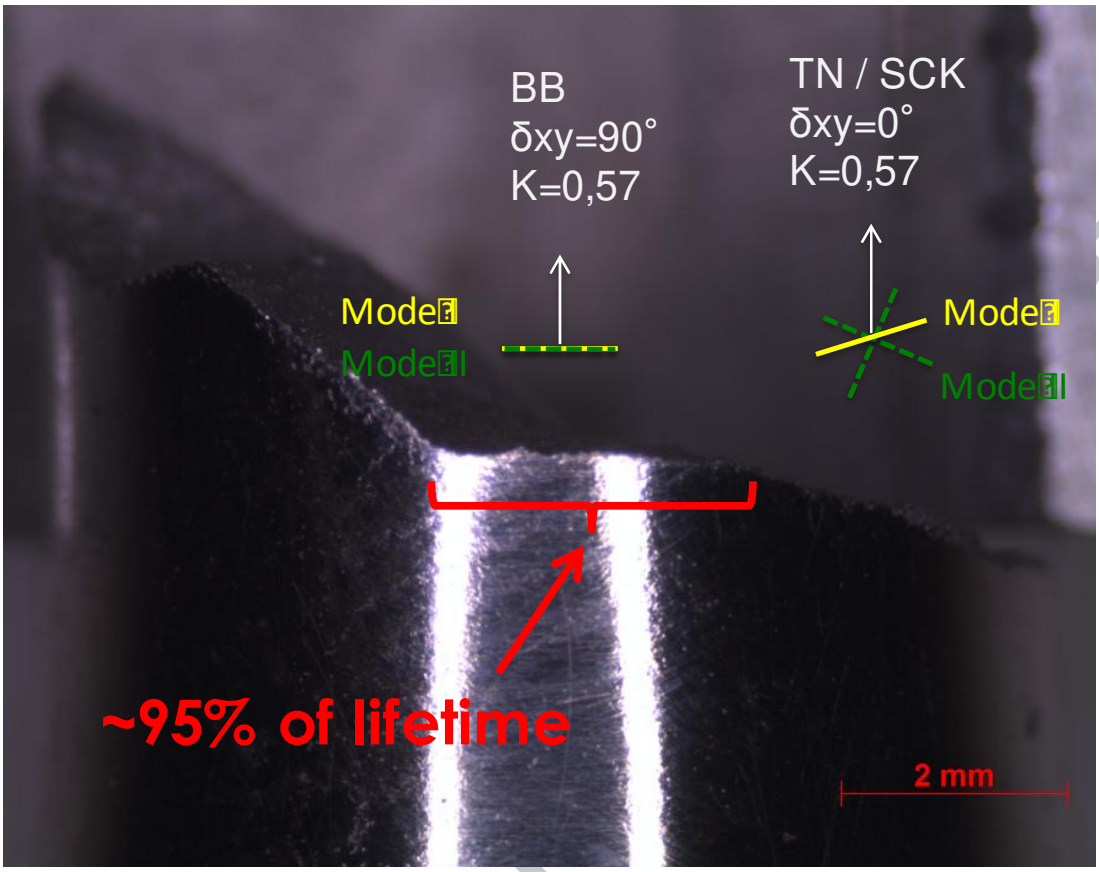

Figure 4 Fatigue crack after failure / specimen 525_9_REPLICA

3.3 Crack growth kinetics

In spite of the three-dimensionality of the crack, the surface length is a relevant quantity to characterize the damage state during specimen lifetime [31,33,34].

Figure 5 shows surface crack measures for 525_9_REPLICA specimen.

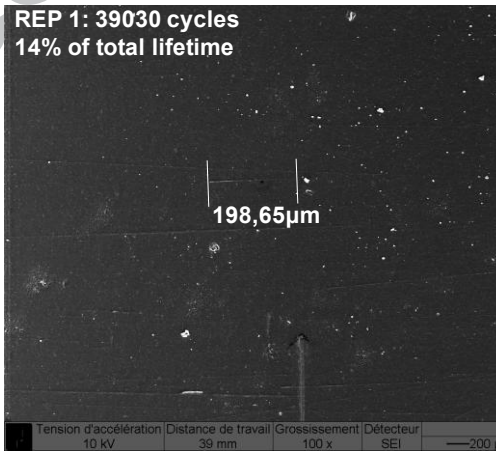

a)

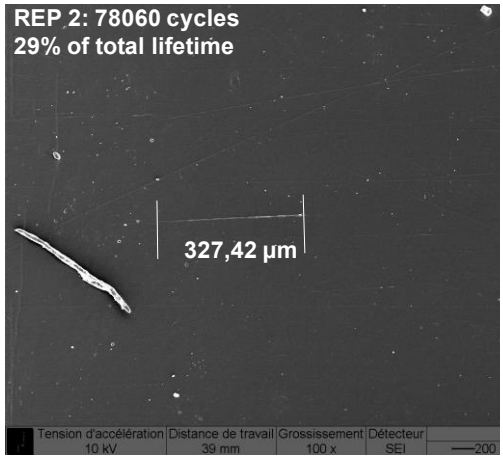

b)

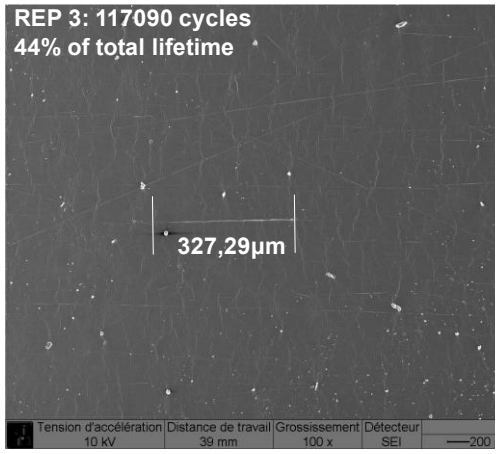

c)

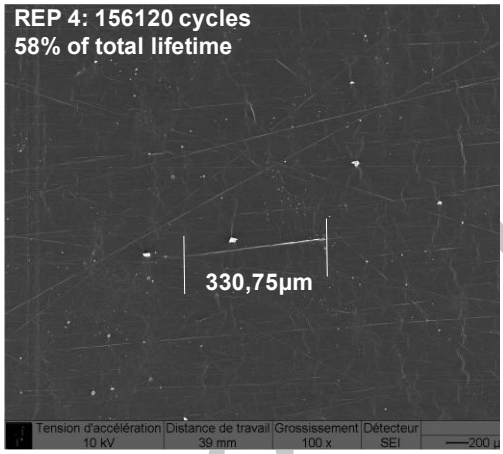

d)

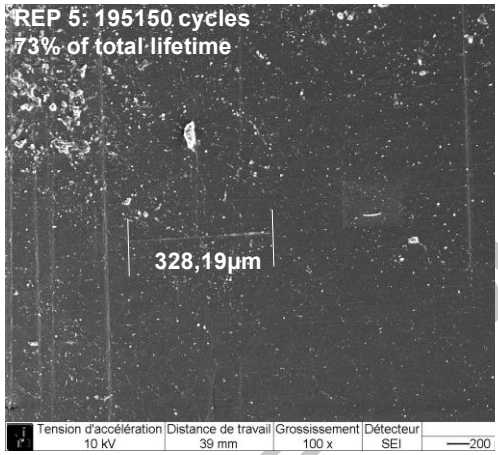

e)

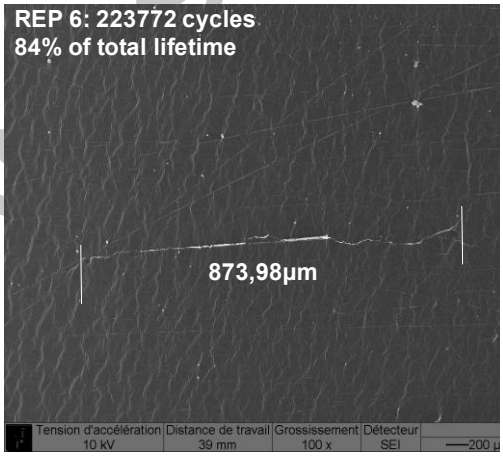

f)

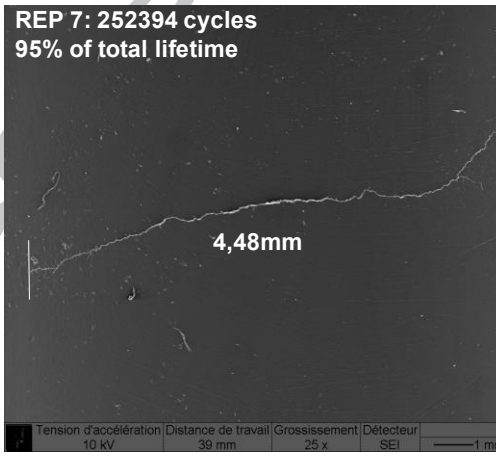

g)

Figure 5 SEM surface observation of the evolution of the main crack through lifetime (specimen 525_9_REPLICA)

In order to further characterize the crack propagation kinetics under the spectrum, Figure 6 displays the crack length (noted *2a*) vs the ratio N/Nf (where N is the current number of cycles and Nf the number of cycles at failure). Different test results are drawn: the blue solid line represents the crack evolution for the full spectrum presented in Figure 1, whereas the three other lines are obtained from tests under constant amplitude (torsion, tension and a multiaxial tension-torsion loading with a stress ratio k=0.5 and a phase shift of 90°). These latter results come from [19], who explain the different kinetics by the damage configuration: in the case of torsion, the homogeneous and diffuse damage leads to a linear evolution, while the localized damage (observed for the other loadcases) is influenced by the microstructure heterogeneity and causes a nonlinear crack propagation evolution. The crack growth kinetics under full spectrum is highly nonlinear. A fast evolution of crack length is observed in the first 30% of lifetime, followed by a plateau until catastrophic failure. This particular behavior may be explained by the influence of the SCK blocks, which accelerate crack growth in the first stage and slow it down by plasticity in a second step. This perturbation may be correlated with the observations by [28] that pointed out the influence of plasticity and crack closure in crack growth kinematics. This possible role of SCK blocks on initial nonlinearity is also supported by the comparison with the multiaxial loading curve. If the effect of the TN blocks is assumed negligible, the spectrum loading is quite close to “90° out-of-phase k=0.5”. Therefore, the SCK blocks seem to be responsible for the initial strong nonlinearity.

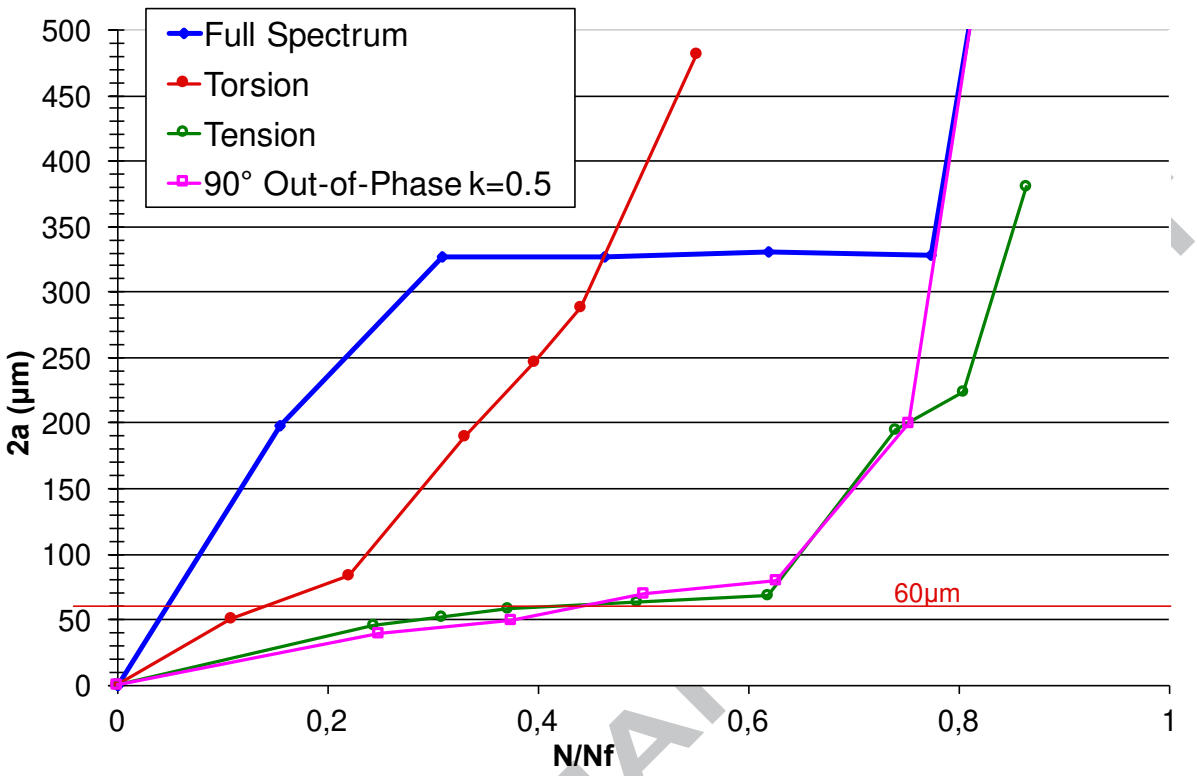

Figure 6 Crack length vs fatigue life ratio for spectrum load compared to constant amplitude load

The red horizontal line in Figure 6 corresponds to 2a=60µm. This length characterizes the required number of cycles for a crack initiated inside a ferrite grain to cross the neighboring pearlite grains, seen as the most important microstructural barrier for this material (Figure 7) [35]. It corresponds at the surface to a ferrite grain + 2 pearlite grains. The "crack initiation length" is independent of loading type, but the duration of this phase is different. This length takes into account micro-plasticity and propagation of micro-cracks [36], and can be seen as the transition between initiation and propagation.

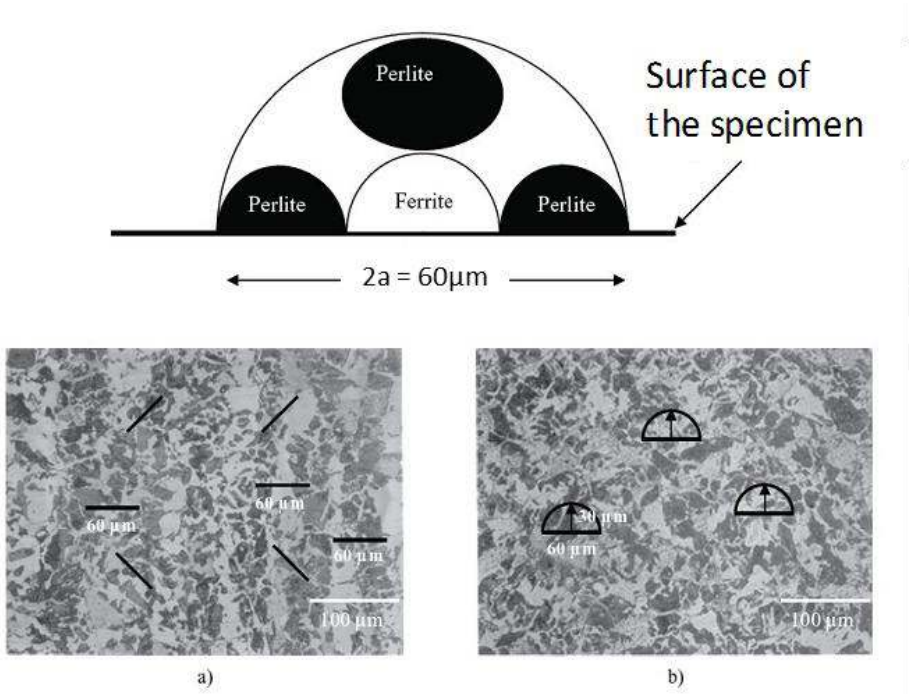

Figure 7 Definition of "initiation length" [35]
a) Longitudinal direction b) Transversal direction

In conclusion, this part provides clues to understand the effect of overloads on 1045 steel specimens. In spite of their limited number, the SCK blocks have a very harmful influence on the total lifetime of the specimen. The lifetime reduction is about 60%. However, these cycles do not seem to influence the critical initiation and propagation planes. The crack initiation is very rapid when the specimen is subject to the variable spectrum and its evolution is highly nonlinear.

4 Lifetime prediction using fatigue criterion methodology

The previous sections analyzed two spectra differing only by the presence of an overload (SCK blocks) each 2600 tension cycles. In this section, the discussion will address fatigue criterion methodology with two different damage accumulation rules: the Miner linear accumulation rule [14] and the "Damage Curve Approach" (DCA) [17]. This latter approach is motivated by its simplicity of use and the fair correlation that can be found in general between the simulations and the experimental results. The fatigue criterion approach is widely

used in industrial contexts. Its numerical processing is very simple and leads to low computer run times. However, a physically motivated criterion has to be selected to capture the main specificities of multiaxial fatigue loading. The problem encountered in this study is the very wide domain, ranging from LCF for the SCK cycles to HCF for the TN ones. In order to maintain the methodology simplicity and optimize CPU time for industrial applications, no plastic correction will be employed for SCK cycles. However, the DCA accumulation rule will be studied in order to take into account nonlinear behavior.

4.1 Multiaxial fatigue criterion

An abundant literature deals with fatigue criteria [1-13]. In this work, the criterion recently proposed [18] is tested by simulating the above described variable amplitude spectrum. It has been found to accurately simulate the fatigue lifetime under different loading cases (in particular non proportional [18]), while being easy to use. It is built from the invariants of the macroscopic stress tensor (same type of approach as [8-11]) and reads as:

$$\sigma_{Vu} = \max_{t\in T}\left\{\sqrt{\gamma_1 J_2'(t)^2 + \gamma_2 J_{2,mean}^2 + \gamma_3 I_f(I_{1,a}, I_{1,m})}\right\} = \beta(N) \quad (5)$$

Equation (5) defines an equivalent stress σ_{vu}. It involves not only the second invariant of the amplitude of the stress deviator $J'_2(t)$ but also the mean value $J_{2,mean}$ of this invariant over the period. This latter term has been found to capture the phase shift effect in a simple way. The term I_f is a function of the amplitude ($I_{1,a}$) and of the mean value ($I_{1,m}$) of the hydrostatic stress. The expression of I_f depends on the type of material and can be found in [18]. For a given loading, the maximum value of σ_{vu} is calculated during a period and compared with the value of $\beta(N)$, a characteristic parameter depending on the number of cycles (in order to assess the finite failure stress level). The four parameters of the criterion (γ_1, γ_2, γ_3, β) can be identified from two fatigue limits (for example, fully reversed torsion and tension) and the ultimate strength. The expression (5) is also capable of taking into account the different effects of phase shift (increase or decrease of the fatigue limit, depending on the material). The complete identification procedure can be found in [18]. For the 1045 steel, it leads to the values presented in Table 4.

Table 4 Fatigue criterion parameters for 1045 steel

γ_1	γ_2	γ_3 (MPa)	$I_f\left(I_{1,a}, I_{1,m}\right)$	β (MPa)
0,65	0,8636	39	$I_f\left(I_{1,a}, I_{1,m}\right) = I_{1,a} + I_{1,m}$	169

When extension to finite lifetimes is needed, an optimal S-N curve should include experimental data from this whole range, but in the absence of such results a standard Basquin formulation, identified here on fully reversed torsion, is used as reference S-N curve. Figure 8 plots the experimental Vu equivalent stress (5) vs. the fatigue lifetime and the corresponding Basquin interpolation [37].

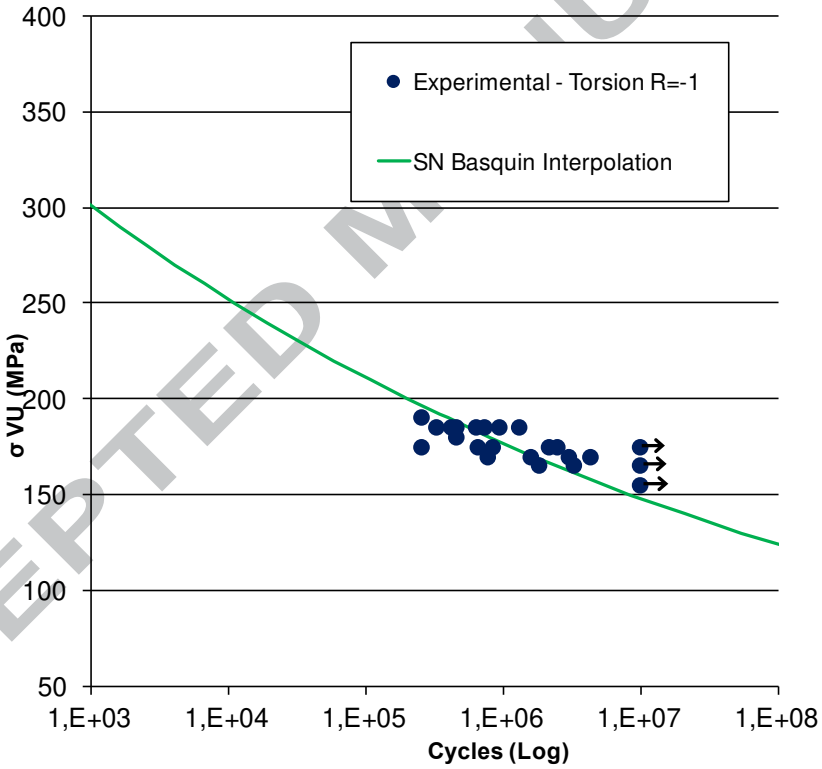

Figure 8 Basquin interpolation, experimental torsion R=-1

Basquin law (6) is identified by linear regression considering the equivalent stress σ as independent variable (ISO12107, [38]). An example of identification can be found in [39]. All simulations are performed using the SN curve with 50% of survival probability and 50% of confidence interval. The identification leads to the following equation of the Basquin curve:

$$N = \frac{1.53.10^{35}}{\sigma^{12.982}} \qquad (6)$$

4.2 Damage accumulation rule

Once the fatigue criterion is selected and material parameters are identified, an accumulation rule has to be chosen in order to deal with variable amplitude loads. In this work, two usual rules are compared: the Miner linear accumulation rule [14] and the "Damage Curve Approach" (DCA) [17]. This latter approach is motivated by its simplicity of use and the fair correlation that can be found in general between the simulations and the experimental results.

4.2.1 Miner's linear damage accumulation rule

Firstly, the multiaxial fatigue criterion [18] is combined with the classical Miner's linear damage accumulation rule [14] to predict fatigue life of both full spectrum and « no shocks spectrum ». In order to illustrate the performance of the proposed criterion, the same analysis will be performed using the reference Crossland criterion [8].

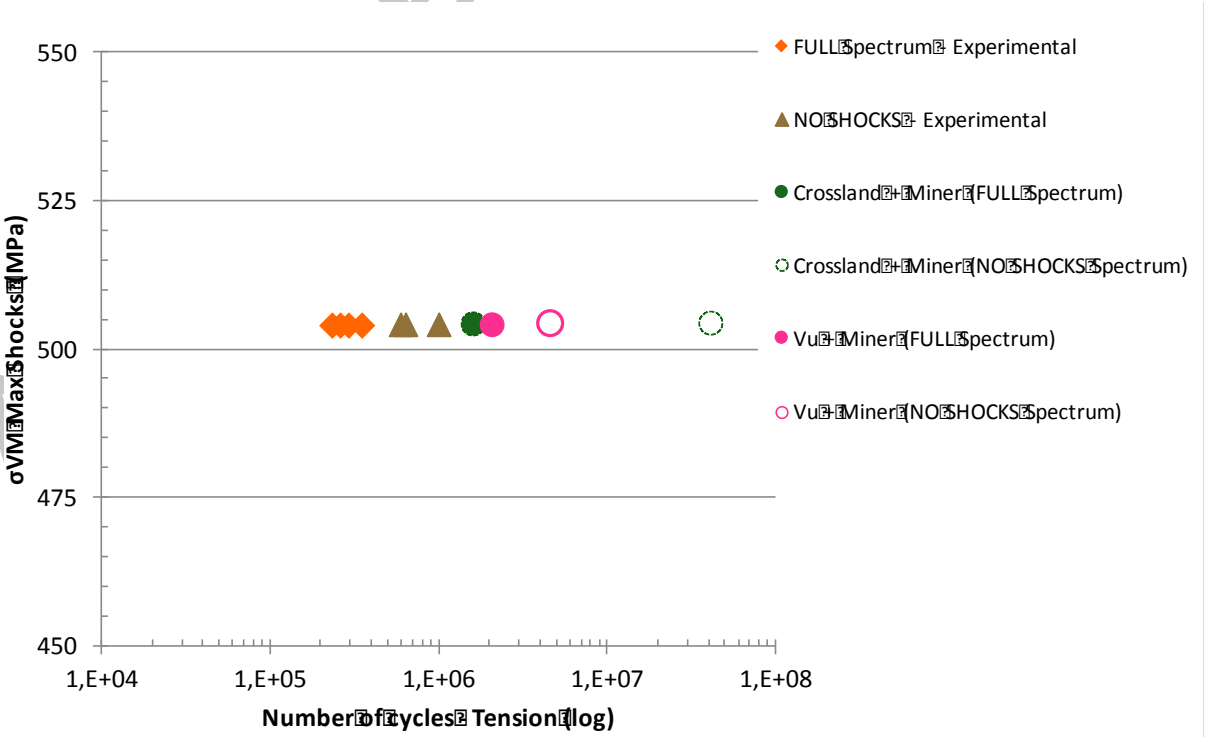

Figure 9 Crossland and Vu criteria with Miner's accumulation rule prediction for

full and "no shocks" spectra.

Figure 10 compares numerical and experimental results for "FULL" spectrum and "NO SHOCKS" spectrum. Several conclusions can be drawn:

- As regards the prediction of fatigue lifetime for full spectrum, both approaches give similar results. The general tendency is non-conservative when compared with experimental data.
- The non-conservative tendency is also observed for "NO SHOCKS" spectrum simulations. However, the proposed criterion seems to better predict the gap between fatigue lifetime of full spectrum and "NO SHOCKS" spectrum.

It is important to note that the methodology combining a fatigue criterion and the linear accumulation rule is pushed to its limits when applied to full spectrum. Indeed, the full spectrum covers a wide range of stress levels, varying from elasticity for BB and TN, and plasticity for SCK.

4.2.2 Damage Curve Approach

In a second step, the fatigue criterion (5) is associated with a nonlinear damage accumulation rule. The Miner's rule is compared with a simple non-linear cumulative damage rule, the Damage Curve Approach (DCA) [17]. This latter approach is governed by Equation (7), providing the damage level as a function of the current number of cycles n and the number of cycles at failure N_f

$$D = \left(\frac{n}{Nf} \right)^{(Nf)^{\alpha}} \qquad (7)$$

The non-linearity is a consequence of the parameter α (the higher α, the more nonlinear the accumulation), which is experimentally identified. Its value is determined by the means of tests exhibiting the nonlinearity of damage accumulation, for example uniaxial tension - torsion block loadings [19]. Two loading sequences are carried out: (i) a given number of alternate tension cycles is applied and then the specimen is subjected to alternate torsion up to failure, (ii) a given number of alternate torsion cycles is applied and then the specimen is subjected to alternate tension up to failure. Experimental results are plotted in

Figure 10: whereas the Miner linear accumulation rule is represented by the dashed line, the test data show a nonlinear accumulation. The parameter α controls this non linearity.

However, the experimental points presented in Figure 10 are very irregular and no clear tendency can be identified. This irregularity may come from a strong influence of microstructure. The identification of α is performed by creating an envelope of experimental points. The estimated lifetime using DCA is higher than the lifetime obtained from the linear accumulation of Palmgren - Miner ($(\frac{n}{Nf})_{Ta} + (\frac{n}{NF})_{To} = 1$) in the case of tension - torsion ($\sum \frac{n}{Nf} > 1$) and lower in the case of torsion - tension ($\sum \frac{n}{Nf} < 1$). Those predicted tendencies are in agreement with several experimental results including the observations in [33] for 1045 steel and in [40], for S45C steel. A value of α=0,6 is found to be fairly satisfactory to forecast the experimental data.

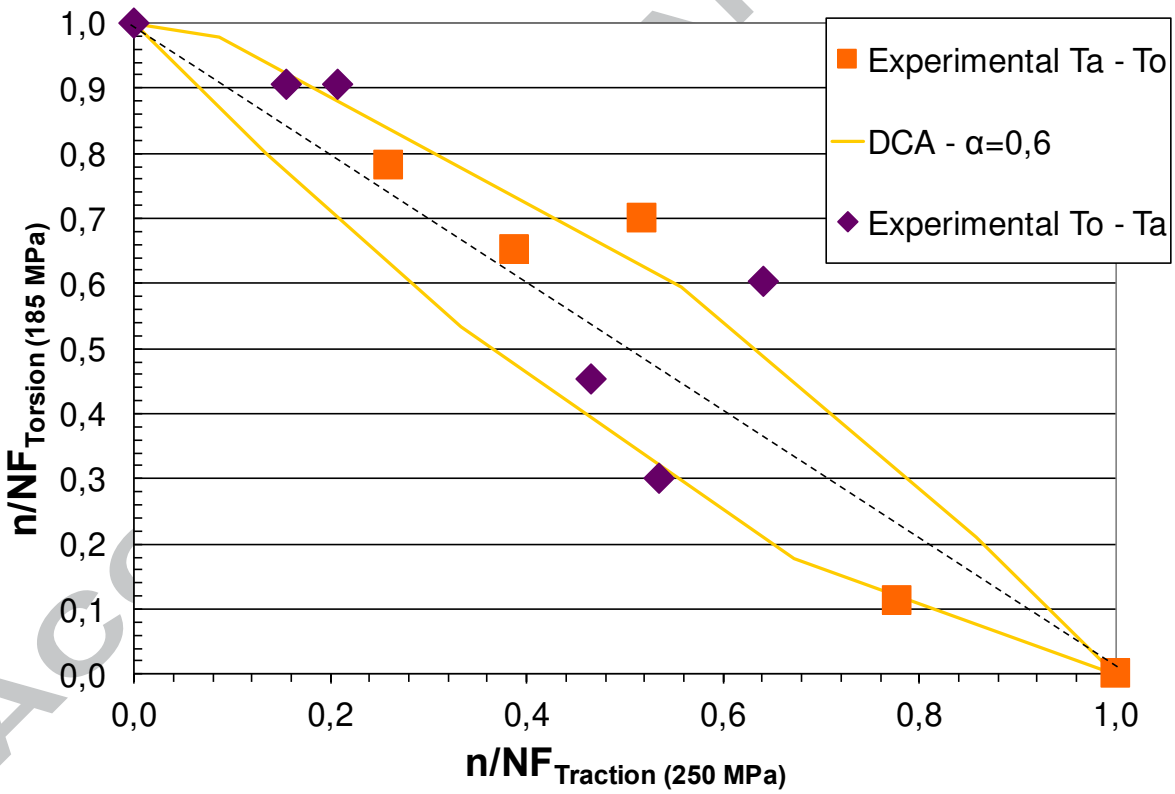

Figure 10 Tension (Ta) – torsion (To) block loading: experimental results and identification of parameter α

Figure 11 compares numerical and experimental results for "FULL" spectrum and "NO SHOCKS" spectrum. Several conclusions can be drawn:

- The linear damage accumulation predicted by Miner's rule together with the Vu criterion is not sufficient to accurately represent fatigue lifetime for both "FULL" and "NO SHOCKS" spectrum, the fatigue lifetime is strongly overestimated
- The nonlinear accumulation DCA approach (with α =0.6) substantially improves the simulation for "FULL" spectrum.
- The DCA approach and the Miner's rule provide very similar results in the "NO SHOCKS" case.
- From the previous point, it can be concluded that the value of α=0,6 is valid only for the "FULL" spectrum and cannot be transposed for "NO SHOCKS" spectrum. The methodology seems to be suited to loadings involving strong stress level variations. A modification of the value of α could be a simple and tractable solution. Indeed, the evolution of damage accumulation is probably different according fatigue domains and then different values are needed for α.

It is important to note that no plastic correction is applied in order to maintain methodology simplicity and optimize CPU time. The non-linearity induced by shocks plasticity is taken into account only by DCA accumulation rule.

None of the methodologies presented in this section (fatigue criterion + linear or nonlinear damage accumulation rule) is capable of accurately simulate simultaneously the fatigue lifetimes of samples subject to a loading spectrum with and without overloads. In order to overcome this difficulty, the next section presents a more complex method: the damage evolution is simulated by a two-scale model written in the framework of the Continuum Damage Mechanics (CDM).

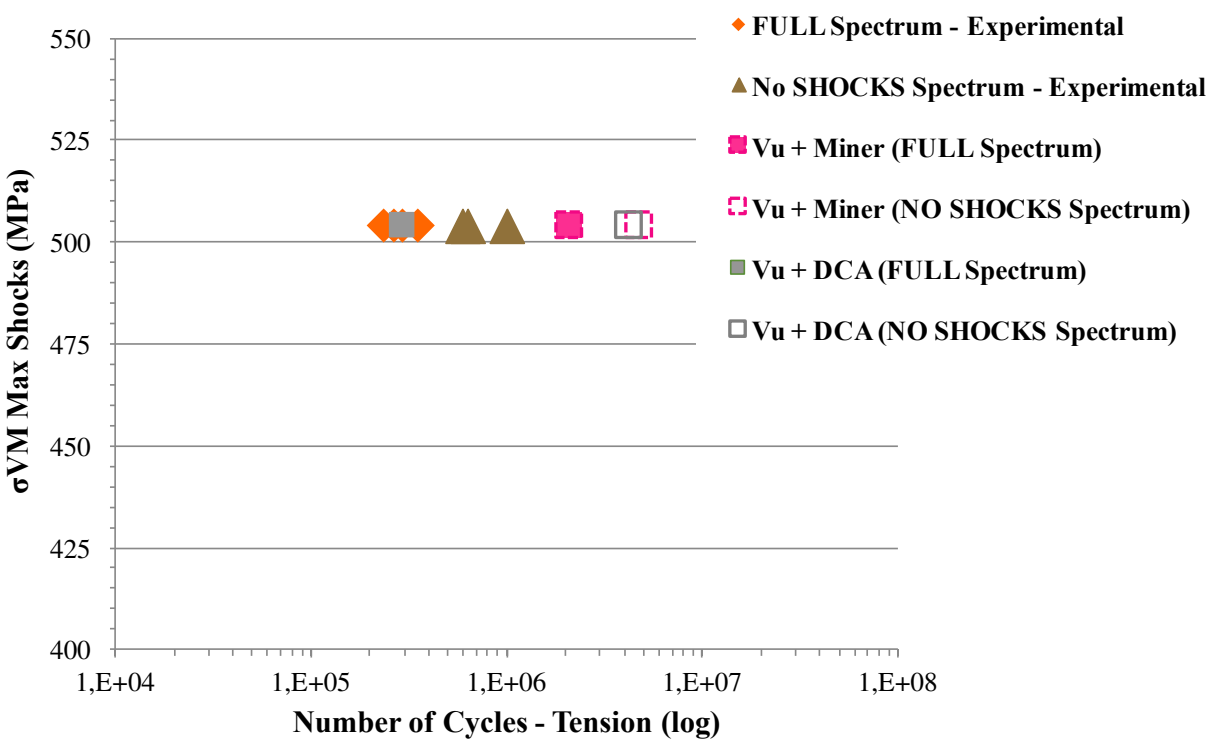

Figure 11 Comparison of cumulative damage rules: linear vs. non- linear

5 An elastic-plastic damage model for lifetime prediction in HCF regime with overloads

5.1 An elastic-plastic damage model for HCF life predictions

In this section, a two-scale damage model dedicated to multiaxial HCF is presented. This model has been proposed in [19], and only the main features are briefly recalled in this section. In HCF, the main source of failure of metallic components is attributed to plasticity and damage at grain scale (micro/mesoscopic scale). This argument is the starting point for many multi-scale models which can be found in the literature. For example, [1] proposed a non-initiation criterion at microscopic scale. However, loading on structure is applied at macroscopic scale, justifying the choice of a two-scale modelling framework which is nowadays widely found in the literature [23,41-44].

The crack initiation process is the result of a simple slip system within one or many grains. This assumption is consistent with observations carried out on different materials [45]. The link between the stress at macroscale $\underline{\underline{\Sigma}}$ and at microscale $\underline{\underline{\sigma}}$ is given by the classical Lin-Taylor localization relationship $\underline{\underline{\sigma}} = \underline{\underline{\Sigma}} - 2\mu\underline{\underline{\varepsilon}}^{p}$ (where μ is the shear modulus and $\underline{\underline{\varepsilon}}^{p}$ the plastic strain at the grain scale). The model is formulated in the rigorous framework of irreversible thermodynamics with internal variables for isothermal, time-independent and small deformation transformations. The evolution of internal variables is governed by: (i) one (or many) threshold function(s) answering the question "when do plasticity and damage evolve?" and (ii) one (or many) dissipation potential(s) indicating, by assumption of normality, how progress this mechanisms [46]. The main ingredients of the model are briefly recalled below.

Together with the plastic strain $\underline{\underline{\varepsilon}}^{p}$, the isotropic hardening (p) and kinematic hardening ($\underline{\underline{\alpha}}$) variables, a scalar damage variable d is used to account for the evolution of microcracks at the grain scale. This "damage effect variable" acts on the degradation of the mechanical strength of crystal that affects directly the isotropic hardening.

Regarding the evolution laws of the plastic variables, the yield surface is based on the criterion presented in Section 4, in order to benefit from its capacity to account for the specificities of HCF loadings. The rates of the plastic variables follow the normality rule with respect to a dissipation potential different from the plastic yield surface and whose expression can be found in [19].

The damage evolution law $\dot{d}$ is split into two different expressions in order to account for the initiation and propagation phases:

$$\begin{aligned} \dot{d} &= \dot{d}_{initiation} \text{ if } d \leq d_p \\ \dot{d} &= \dot{d}_{propagation} \text{ if } d > d_p \end{aligned} \qquad (8)$$

where d_p is the damage threshold of propagation phase. Moreover, the expression of $\dot{d}_{propagation}$ directly involves, as a parameter, the hydrostatic part of the stress at the microscale in order to distinguish tension and torsion. The damage evolution laws are governed by the normality rule applied to a dissipation potential and are specified in [19]. The step-by-step integration of (8) leads to nonlinear damage accumulation. Failure occurs when the damage variable d reaches the critical value d_c.

5.2 Comments on Vu et al. model and extension to account for overload

The assessment of the model briefly recalled above has been carried out for multiaxial, proportional, out-of-phase and block loadings in [19]. The obtained results prove that the model is efficient for simulating HCF lifetimes. The model is implemented in the rigorous framework of irreversible processes that allows an explicit description of the incremental evolutions of plastic and damage variables. The use of a two scale approach (mesoscopic–macroscopic) enables to capture physical processes of material degradation (plasticity, damage) at the grain scale. In addition, several proper effects of HCF are taken into account including fatigue damage accumulation below the fatigue limit, mean stress and phase shift effects. The model describes the nonlinear damage accumulation thanks to the distinctions of two damage mechanisms (tension/torsion) and two phases of crack growth (different damage evolution law for initiation and propagation). The model allows hence fairly good prediction of S–N curves for both proportional and non-proportional multiaxial loadings at constant amplitude, with and without mean stress. For variable amplitude loadings, the model proved also its efficiency in dealing with block loadings.

The model, which is dedicated to multiaxial HCF, cannot describe correctly high amplitude fatigue loading (overload) falling in low cycle fatigue (LCF) regime. In order to deal with the overloading SCK cycles of the spectrum presented in Figure 1, the plastic yield stress needs to be modified.

The plastic yield surface of the original model reads as follows:

$$f\left(\underline{\underline{\sigma}},\underline{\underline{x}},r\right)=\sqrt{\gamma_1 J_2^2\left(\underline{\underline{\sigma}}-\underline{\underline{x}}\right)+\gamma_2 J_{2,mean}^2+\gamma_3 I_f\left(I_{1,a},I_{1,m}\right)}-\left(r+r_0\right)\le 0 \quad (9)$$

where J_2 is the second invariant of the deviator of $\underline{\underline{\sigma}}-\underline{\underline{x}}$, $J_{2,mean}$ the mean value over the period of the second invariant of the amplitude of the stress tensor and I_f a function of the amplitude ($I_{1,a}$) and of the mean value ($I_{1,m}$) of the hydrostatic stress. The real r_0 is the initial radius of the yield surface. The tensor $\underline{\underline{x}}$ is the backstress associated to the kinematic hardening variable $\underline{\underline{\alpha}}$. The function r governs the isotropic hardening. It is supposed to tend towards an asymptotic value $\tilde{r}_\infty$ when the accumulated plastic strain p increases:

$$r=\tilde{r}_\infty\left(1-\exp(-gp)\right)\exp\left(-sd\right) \quad (10)$$

where g is the isotropic hardening modulus. The parameter s is the damage sensitivity modulus and the term $\exp(-sd)$ shows the competition between plasticity and damage at local scale.

The terms $J_{2,mean}$ and $I_f(I_{1,a}, I_{1,m})$ are determined directly from the macroscopic stress tensor during a period T while $J_2(\underline{\underline{\sigma}} - \underline{\underline{x}})$ is a mesoscopic quantity according to the local stress tensor $\underline{\underline{\sigma}}$ and the backstress tensor $\underline{\underline{x}}$ at the grain scale. Since $\gamma_1 J_2^2(\underline{\underline{\sigma}} - \underline{\underline{x}})$ is positive, the applied macroscopic load must verify the following inequality:

$$\sqrt{\gamma_2 J_{2,mean}^2 + \gamma_3 I_f(I_{1,a}, I_{1,m})} \leq (r + r_0) \quad (11)$$

During the very first loading cycles, when the accumulated plastic strain p is very low, the value of r is close to zero resulting in:

$$\sqrt{\gamma_2 J_{2,mean}^2 + \gamma_3 I_f(I_{1,a}, I_{1,m})} \leq r_0 \quad (12)$$

Inequality (12) imposes a strong restriction on the load level and prevents from dealing with SCK overloads, when the values of $J_{2,mean}$ and I_f are too high and violates (12). In order to extent the application range of the model to LCF, the expression of the yield surface is slightly modified:

$$f(\underline{\underline{\sigma}}, \underline{\underline{x}}, r) = \sqrt{\gamma_1 J_2^2(\underline{\underline{\sigma}} - \underline{\underline{x}}) + \gamma_2 J_{2,mean}^2 + \gamma_3 I_f(I_{1,a}, I_{1,m})} - A.(r + r_0) \leq 0 \quad (13)$$

with

$$A = 1 + \left\langle \frac{\sigma_{eq}^0}{r_0} - 1 \right\rangle \text{ and } \sigma_{eq}^0 = \sqrt{\gamma_2 J_{2,mean}^2 + \gamma_3 I_f(I_{1,a}, I_{1,m})} \quad (14)$$

The parameter A can be seen as an expansion coefficient of the yield surface when switching from HCF to LCF. The Macaulay brackets <…> (<x>=x if x>0, <x>=0 otherwise) modify the value of A when the loading level suddenly increases:

- in HCF domain, for low loading levels ($\sigma_{eq}^{0} \le r_0$), $A = 1$
- In LCF domain, for high loading levels ($\sigma_{eq}^{0} > r_0$): $A = \dfrac{\sigma_{eq}^{0}}{r_0} > 1$

In LCF, the yield surface radius is magnified and it is restored to its initial value when switching to HCF. In this latter case, the expression of the plastic yield surface remains the same as (9). The value of the expansion parameter A is directly determined from the macroscopic invariants $J_{2,mean}$ and I_f and does not require the identification of an extra material constant. The evolution laws of the internal plastic variables ($\underline{\underline{\varepsilon}}^{p}$, $\underline{\underline{\alpha}}$, p) and of the damage variable d are not modified with respect to [19].

5.3 Assessment of improved model

In this section, the improved model is tested by simulating some usual multiaxial loading cases as well as the variable amplitude spectrum (Figure 1). The model parameters for the 1045 steel mentioned in this section have been identified in [19], and are recalled in Table 5. The identification procedure requires three material properties (fatigue limits under fully reversed tension and torsion, ultimate strength), two S–N curves (reversed torsion, reversed tension) and one curve giving the crack length growth under reversed tension loading.

Table 5 Model parameters for the 1045 steel

μ (MPa)	γ_1	γ_2	γ_3	r_0 (MPa)	$\tilde{r}_\infty$ (MPa)	g	s	d_p	d_c
70000	0.65	0.8636	39	160	9	0.1	0.1	0.1	1

In a first stage, the model is used to simulate constant amplitude loadings. Whereas [19] only simulated S-N curves in the HCF regime (more than 100,000 cycles), the introduction of the expansion coefficient A≠1 allows now to extend the cycle range. The S-N curves predicted by the improved model are shown in Figure 12. It can be seen that the transition from the original version of the model (A=1) to LCF domain is quite smooth under both reversed torsion and reversed tension loadings. The yield surface modification does not introduce artificial discontinuities, the HCF curve is continued towards the lower numbers of cycles. Of course this approach would need modifications for very small number of cycles (less than 10 000)

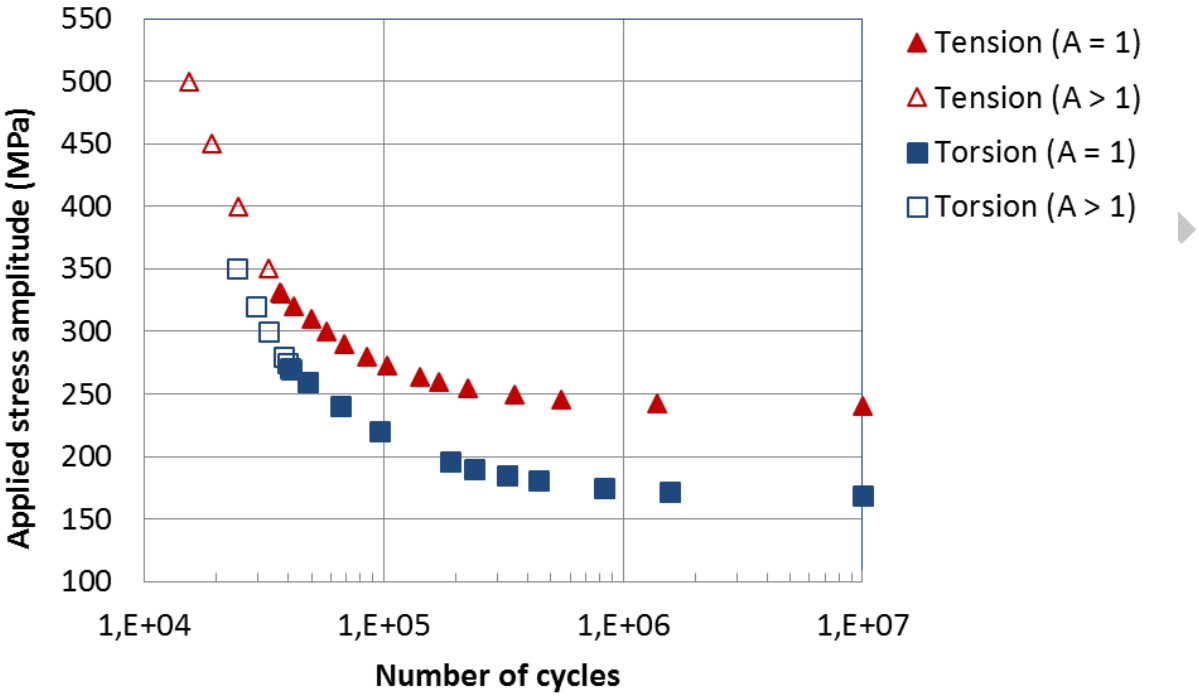

Figure 12 Simulated S-N curve under reversed constant amplitude loadings

Table 6 summarizes the results predicted by the improved version of the model for the variable spectra mentioned in Table 2. The simulated lifetimes of the specimens subject to full spectrum are in good agreement with the experimental results and are of the same order of magnitude as those obtained by the approach "criterion + nonlinear accumulation rule" (Figure 11). The main improvement regards the simulation of the lifetime of specimens undergoing spectra without SCK blocks. Whereas the criterion approach predicted failure after 4,000,000 cycles, the damage model provides a lifetime closer to the experimental results, moreover in a conservative way. This methodology is more complex to implement but allows to cover a wide range of lifetime.

Table 6 Predicted results for Automobile Spectra

Specimen Reference	σvm Shock Theoretical Value [MPa]	σvm Shock Experimental Value [MPa]	Experimental number of tension cycles at failure	Predicted number of tension cycles at failure
525_1	525	504	234 180	**276 086**
525_2	525	504	353 872	
525_3	525	504	294 026	
525_9_REPLICA	525	504	265 404	
600_6	600	526	124 896	**119 809**
600_7	600	526	140 508	
480_5	480	463	801 416	**1 234 582**
480_8	480	463	629 648	
525_10_NO-SHOCKS	525	504	596 544	**329 815**
525_11_NO-SHOCKS	525	504	638 560	
525_12_NO-SHOCKS	525	504	1 004 432	

6 Conclusion

The goal of this work was to compare different methodologies dedicated to the determination of fatigue lifetime of industrial components subjected to complex multiaxial spectra. For decades, an abundant literature is dealing with a wide variety of approaches, from simple fatigue criteria to damage models, via different accumulation rules. However, little work has been done to rigorously compare these different approaches on the basis of complex loads representative of real use conditions. To this end and for ease of comparison, the work presented here focused on a unique material, a 1045 carbon steel, whose samples have been subjected to a loading spectrum used in tension-torsion tests and designed to represent real fatigue loadings undergone by in-service automotive structures. This spectrum involves several sequences with different load ratios, phase shifts and maximum stress levels. In particular, it includes overloads which are responsible for local plasticity. The lifetime has

been measured for different stress levels. Thanks to the observations of fracture surfaces and of crack length, a strongly non linear damage evolution has been identified.

This experimental database is the starting point for the evaluation of different simulation tools to predict fatigue lifetime under complex multiaxial spectra. Because of their ease of use, two criteria built from stress invariants have been selected (Crossland and Vu) and associated to two accumulation rules (linear and nonlinear). The linear damage accumulation proves not reliable enough, even in the case of the Vu criterion which takes into account the multiaxiality character of the loading spectrum. The nonlinear accumulation DCA approach is a simple way to substantially improves the simulation.

However, the methodology consisting in the association of a fatigue criterion and a damage accumulation rule (even nonlinear) fails to accurately simulate the fatigue lifetimes of samples subject to a loading spectrum involving overloads. This issue can be overcome by simulating damage evolution by the means of the damage model proposed by Vu [19] slightly modified in order to take into account cycles exceeding the macroscopic yield stress. This extension does not need the identification of any extra parameter compared to the original version of the model and improves its prediction. The computation time is however the price to pay for this reliability of the results: whereas the calculation “fatigue criterion + DCA” is quasi instantaneous when using a standard personal computer, the incremental approach of the damage model leads to quite high computation times (about 30 minutes for a simulation of 500 000 cycles on one material point).

Work in progress aims at extending the methodology to fully random spectra. To this end, a specific methodology has to be developed to determine the stress invariants involved in the Vu yield surface when no time period can be defined.

ACKNOWLEDGMENTS

This research is funded by Renault and Vietnam National Foundation for Science and Technology Development (NAFOSTED) under grant number 107.02-2014.25

This work pertains to the French Government program “Investissements d’Avenir” (LABEX INTERACTIFS, reference ANR-11-LABX-0017-01).

REFERENCES

[1] Dang Van, K. (1973). Sur la résistance à la fatigue des métaux. Sciences et Technique de l'Armement, 47(3), 641–722.

[2] Findley, W. (1958). A theory for the effect of mean stress on fatigue of metals under combined torsion and axial load or bending. ASME J Eng Ind, 301–306

[3] McDiarmid, D. (1991). A general criterion for high cycle multiaxial fatigue failure. Fatigue and Fracture of Engineering Materials and Structures, 14(4), 429-453

[4] Robert, J. L. (1992). Contribution à l'étude de la fatigue multiaxiale sous sollicitations périodiques ou aléatoires. PhD thesis, INSA Lyon.

[5] Papadopoulos, I. (1994). A new criterion of fatigue strength for out-of-phase bending and torsion of hard metals. International Journal of Fatigue, 16(6), 377–384.

[6] Papuga, J., and Růžička, M. (2008). Two new multiaxial criteria for high cycle fatigue computation. International Journal of Fatigue, 30(1), 58-66.

[7] Zenner, H., Simbürger, A., and Liu, J. (2000). On the fatigue limit of ductile metals under complex multiaxial loading. International Journal of Fatigue, 22(2), 137-145

[8] Crossland, B. (1956). Effect of large hydrostatic pressures on the torsional fatigue strength of an alloy steel. Proc. Int. Conf. on Fatigue of Metals, London, UK

[9] Li, B., Santos, J., and Freitas, M. (2001). A computerized procedure for long- life fatigue assessment under complex multiaxial loading. Fatigue and Fracture of Engineering Materials and Structures, 24(3), 165-177

[10] Mamiya, E., Araújo, J., and Castro, F. (2009). Prismatic hull: a new measure of shear stress amplitude in multiaxial high cycle fatigue. International Journal of Fatigue, 31(7), 1144-1153

[11] Sines, G. (1959). Behaviour of metals under complex static and alternating stresses. (G. Sines and J. Waisman, Eds.). New York: Mc Graw Hill.

[12] Ellyin, F., and Xia, Z. (1993). A general fatigue theory and its application to out-of-phase cyclic loading. ASME Journal of Engineering Materials and Technology, 115(4), 411-416

[13] Palin-Luc, T., and Lasserre, S. (1998). An energy based criterion for high cycle multiaxial fatigue. European Journal of Mechanics-A/Solids, 17(2), 237-251

[14] Miner, M. (1945). Cumulative damage in fatigue. Journal of Applied Mechanics, 67, A159-A164

[15] Chaboche, J.-L. (1974). Une loi différentielle d'endommagement de fatigue avec cumulation non linéaire. Revue Française de Mecanique, 50-51, 71-82

[16] Chaboche, J.-L., Kanouté, P., and Kaminski, M. (2009). Extension and application of a nonlinear fatigue damage accumulation rule for variable amplitude loading programs. In 2nd International Conference on Material and Component Performance under Variable Amplitude Loading, Darmstadt, Germany

[17] Manson, S., and Halford, G. (1981). Practical implementation of the double linear damage rule and damage curve approach for treating cumulative fatigue damage. International Journal of Fracture, 17(2), 169–192

[18] Vu, Q., Halm, D., and Nadot, Y. (2010). Multiaxial fatigue criterion for complex loading based on stress invariants. International Journal of Fatigue, 32, 1004-1014

[19] Vu, Q., Halm, D., and Nadot, Y. (2014). High cycle fatigue of 1045 steel under complex loading: Mechanisms map and damage modelling. International Journal of Damage, 23(3), 377-409

[20] Billaudeau, T. (2002). Fatigue multiaxiale des matériaux à défaut: mécanismes et critère d'endurance, Phd thesis, ENSMA

[21] Billaudeau, T., Nadot, Y., and Bezine, G. (2004). Multiaxial fatigue limit for defective materials: mechanisms and experiments. Acta Materialia, 52(13), 3911–3920

[22] Flaceliere, L., Morel, F., and Dragon, A. (2007a). Competition between mesoplasticity and damage under HCF–Elasticity/damage shakedown concept. International Journal of Fatigue, 29(12), 2281-2297

[23] Flaceliere, L., Morel, F., and Dragon, A. (2007b). Coupling between mesoplasticity and damage in high-cycle fatigue. International Journal of Damage, 16(4), 473-509

[24] Nadot, Y., and Billaudeau, T. (2006). Multiaxial fatigue limit criterion for defective materials. Engineering Fracture Mechanics, 73(1), 112–133.

[25] Palin- Luc, T., Sellier, E., d'Errico, F., andVanhaeren, M. (2002). Elastomer and resin replicas for SEM observation of metallic materials. Experimental Techniques, 26(3), 33-37

[26] Zheng, X.-L. (1995). Overload effects on fatigue behaviour and life prediction of low-carbon steels. International Journal of Fatigue, 17(5), 331-337

[27] Sonsino, C.M. (2001). Interpretation of overload effects under spectrum loading o fwelded high-strength steel joints. Welding in the World, 55, 66-78.

[28] Bonnen, J. J. F., Conle, F., and Topper, T. H. (2001). The role of in-phase and out-of-phase overloads on the torsional fatigue of normalized SAE-1045 steel. International Journal of Fatigue, 23, 385–394

[29] Morel, F., and Huyen, N. (2008). Plasticity and damage heterogeneity in fatigue. Theoretical and Applied Fracture Mechanics, 49(1), 98-127

[30] Suresh, S. (1998). Fatigue of Materials, Cambridge University Press.

[31] Verreman, Y., and Guo, H. (2007). High-cycle fatigue mechanisms in 1045 steel under non- proportional axial-torsional loading. Fatigue and Fracture of Engineering Materials and Structures, 30(10), 932-946

[32] Karolczuk, A., and Macha, E. (2005). A review of critical plane orientations in multiaxial fatigue failure criteria of metallic materials. International Journal of Fracture, 134(3), 267-304

[33] Miller, K. J. (1993). Materials Science Perspective of Metal Fatigue Resistance. Materials Science and Technology, 9, 453–462.

[34] Ohkawa, I., and Takahashi, H. (1997). A study on fatigue crack growth under out-of-phase combined loadings. Fatigue and Fracture of Engineering Materials and Structures, 20(6) 929-940

[35] Nasr A., Nadot, Y., Bouraoui, C., Fathallah, R., Jouiad, M. (2010) Fatigue initiation in C35 steel: Influence of loading and defect, International Journal of Fatigue, 32, 780-787

[36] Miller, K. (1987). The Behaviour of Short Fatigue Cracks and Their Initiation Part II - A General Summary. Fatigue and Fracture of Engineering Materials and Structures, 10(2), 93–113

[37] Dal Cero Coelho, F. (2014). Maîtrise de la tenue en fatigue des cordons de soudure. PhD thesis, ENSMA

[38] ISO 12107:2012. (2012). Metallic materials — Fatigue testing — Statistical planning and analysis of data.

[39] Statnikov, E., and Muktepavel, V. (2000). Efficiency evaluation of ultrasonic impact treatment (UIT) of welded joints in weldox 420 steel in accordance with the IIW program. Applied Ultrasonics, IIW, 1–30.

[40] Chen, X., Jin, D., and Kim, K. (2006). Fatigue life prediction of type 304 stainless steel under sequential biaxial loading. International Journal of Fatigue, 28(3), 289–299

[41] Doudard, C., Calloch, S., Cugy, P., Galtier, A., and Hild, F. (2005), A probabilistic two-scale model for high-cycle fatigue life predictions, Fatigue Fracture of Engineering Materials and Structures, 28(3), 279-288

[42] Huyen, N., Flaceliere, L., and Morel, F. (2008), A critical plane fatigue model with coupled meso-plasticity and damage, Fatigue and Fracture of Engineering Materials andStructures, 31(1), 12-28

[43] Lemaitre, J., Sermage, J. P., and Desmorat, R. (1999), A two scale damage concept applied to fatigue, International Journal of Fracture, 97(1), 67-81

[44] Monchiet, V., Charkaluk, E., and Kondo, D. (2008), A micromechanical explanation of the mean stress effect in high cycle fatigue, Mechanics Research Communications, 35(6), 383-391.

[45] Rasmussen, K., and Pedersen, O. (1980) Fatigue of copper polycristals at low plastic strain amplitudes,. Acta Metallurgica, 28(11), 1467-1478.

[46] Germain, P., Nguyen, Q. S., and Suquet, P. (1983), Continuum thermodynamics, ASME, Journal of Applied Mechanics, 50, 1010-1020

Highlights

- Fatigue lifetimes of samples subjected to complex multiaxial spectrum are measured
- Different simulation tools to predict fatigue lifetime are evaluated
- Incremental damage model can forecast lifetime with and without overload